BMC Cancer

RESEARCH

Open Access

# Epigenomic perturbation of novel *EGFR* enhancers reduces the proliferative and invasive capacity of glioblastoma and increases sensitivity to temozolomide

Craig A. Vincent[1,2], Itzel Nissen[1,2], Soran Dakhel[1,2], Andreas Hörnblad[1] and Silvia Remeseiro[1,2*]

## Abstract

**Background** Glioblastoma (GB) is the most aggressive of all primary brain tumours and due to its highly invasive nature, surgical resection is nearly impossible. Patients typically rely on radiotherapy with concurrent temozolomide (TMZ) treatment and face a median survival of ~ 14 months. Alterations in the Epidermal Growth Factor Receptor gene (*EGFR*) are common in GB tumours, but therapies targeting EGFR have not shown significant clinical efficacy.

**Methods** Here, we investigated the influence of the *EGFR* regulatory genome on GB cells and identified novel *EGFR* enhancers located near the GB-associated SNP rs723527. We used CRISPR/Cas9-based approaches to target the *EGFR* enhancer regions, generating multiple modified GB cell lines, which enabled us to study the functional response to enhancer perturbation.

**Results** Epigenomic perturbation of the *EGFR* regulatory region decreases *EGFR* expression and reduces the proliferative and invasive capacity of glioblastoma cells, which also undergo a metabolic reprogramming in favour of mitochondrial respiration and present increased apoptosis. Moreover, *EGFR* enhancer-perturbation increases the sensitivity of GB cells to TMZ, the first-choice chemotherapeutic agent to treat glioblastoma.

**Conclusions** Our findings demonstrate how epigenomic perturbation of *EGFR* enhancers can ameliorate the aggressiveness of glioblastoma cells and enhance the efficacy of TMZ treatment. This study demonstrates how CRISPR/Cas9-based perturbation of enhancers can be used to modulate the expression of key cancer genes, which can help improve the effectiveness of existing cancer treatments and potentially the prognosis of difficult-to-treat cancers such as glioblastoma.

**Keywords** *EGFR*, Enhancer, Glioblastoma, Epigenomic perturbation, CRISPR/Cas9

## Introduction

Glioblastoma (GB), also known as grade 4 astrocytoma, is a common and highly aggressive type of primary brain tumour, for which survival rates have not significantly improved in recent decades (median survival ~ 14 months, 5-year survival < 5%) [1, 2]. Due to its highly invasive nature, complete surgical resection is nearly impossible [3] and therefore recurrence is inevitable. While the addition of tumour-treating

*Correspondence:
Silvia Remeseiro
silvia.remeseiro@umu.se
[1] Umeå Centre for Molecular Medicine (UCMM), Umeå University, Umeå, Sweden
[2] Wallenberg Centre for Molecular Medicine (WCMM), Umeå University, Umeå, Sweden

© The Author(s) 2023. **Open Access** This article is licensed under a Creative Commons Attribution 4.0 International License, which permits use, sharing, adaptation, distribution and reproduction in any medium or format, as long as you give appropriate credit to the original author(s) and the source, provide a link to the Creative Commons licence, and indicate if changes were made. The images or other third party material in this article are included in the article's Creative Commons licence, unless indicated otherwise in a credit line to the material. If material is not included in the article's Creative Commons licence and your intended use is not permitted by statutory regulation or exceeds the permitted use, you will need to obtain permission directly from the copyright holder. To view a copy of this licence, visit http://creativecommons.org/licenses/by/4.0/. The Creative Commons Public Domain Dedication waiver (http://creativecommons.org/publicdomain/zero/1.0/) applies to the data made available in this article, unless otherwise stated in a credit line to the data.

fields (TTFields) following chemoradiotherapy has led to extended survival [4, 5], the treatment is not widely available due largely to cost-efficiency concerns [6], and in the countries where it is applied, only 30% of patients are eligible and therefore receive this treatment option [7, 8]. Hence, the current standard of care for GB patients consists of radiotherapy and concomitant chemotherapy with temozolomide (TMZ), often preceded by tumour debulking surgery. Temozolomide (TMZ) is a DNA alkylating agent commonly used in the treatment of glioblastoma as adjuvant to radiotherapy. Patients with methylated *MGMT* (O6-methylguanine-DNA methyltransferase) promoter respond with better outcome to TMZ treatment given the role of MGMT in DNA damage repair [9–11], which highlights the relevance of epigenomic cues in the patient outcome upon treatment.

In fact, GB remains a difficult-to-treat cancer due to the high degree of inter- and intra-tumour heterogeneity and the complexity of genetic, epigenetic and microenvironment events. One of the key challenges in treating glioblastoma is the ability of cancer cells to evade the effects of chemotherapy and radiation therapy. This is often due to the over-expression of certain genes, such as *EGFR*, which can promote the survival and proliferation of cancer cells. The Epidermal Growth Factor Receptor gene (*EGFR*) is one of the most frequently altered genes in glioblastoma. 57% of tumours display some form of alteration in *EGFR* [12] and among the classical subtype, *EGFR* is overexpressed in more than 95% [13]. Moreover, high *EGFR* expression in gliomas correlates with reduced overall survival in patients [14]. Constitutive activation of the EGFR signalling pathway can occur through overexpression of the receptor itself or its ligand, through amplification of the *EGFR* locus (which includes non-coding regions), or through coding mutations (e.g. EGFRvIII). All of which result in increased cell proliferation, invasive capacity, survival and angiogenic potential.

While the traditional focus of cancer research has been on the impact of coding mutations, Genome-Wide Association Studies (GWAS) have revealed that most genetic variants that predispose to cancer are located within non-coding genomic regions with potential to act as *cis*-regulatory elements (e.g. enhancers) [15]. Enhancers are stretches of DNA that regulate transcription in a spatiotemporal manner, through their capacity to bind transcription factors (TFs) and protein complexes that control gene expression. In the linear genome, enhancers can be located vast distances from the gene promoter which they act upon, but they require close physical proximity in the 3D nuclear space to exert their regulatory function [16, 17]. Enhancer dysfunction due to genetic, topological or epigenetic mechanisms can contribute to human diseases, including cancer. However, accurate identification of enhancers and understanding their role in disease still remains a challenge [18].

In the context of glioblastoma, the mechanistic contribution of the non-coding regulatory genome to pathogenesis remains understudied. Here, we identify novel *EGFR* enhancer elements in the vicinity of the known GB-associated single nucleotide polymorphism (SNP) rs723527, and we functionally dissect their regulatory potential by introducing CRISPR-based (epi-)genomic perturbations. Targeting these *EGFR* enhancer regions in glioblastoma cells leads to decreased proliferation and migration rates, due in part to an increased rate of apoptosis, which could be triggered by an underlying metabolic reprogramming of these cells. Thus, targeting these novel *EGFR* enhancers diminishes the malignancy of glioblastoma cells by reducing their proliferative and invasive capacity, and sensitising them to treatment with TMZ. Our findings highlight the association between *EGFR* expression and temozolomide efficacy, and demonstrate how CRISPR/Cas9-based targeting of enhancers can be used to modulate the expression of key cancer genes. Combining (epi-)genomic perturbation of enhancers with existing cancer treatments can improve their effectiveness and subsequently the prognosis of glioblastoma and other cancers difficult to treat.

## Methods and materials

### Cell culture

#### *Cell lines*

*U251 MG human glioblastoma cell line* (Sigma-Aldrich, #09063001, authenticated by short tandem repeat (STR)-PCR profiling) were grown in EMEM (EBSS) supplemented with 2 mM Glutamine, 1% NEAA (Non-Essential Amino Acids), 1 mM Sodium Pyruvate, 10% FBS (Fetal Bovine Serum) and 1% penicillin/streptomycin (all from Gibco). HEK293T cells were grown in DMEM/F-12 GlutaMAX™-Supplemented media containing 10% FBS (Fetal Bovine Serum) and 1% penicillin/streptomycin (all from Gibco).

*U3013 human glioblastoma cell line* was established from a GB-patient surgical sample and obtained via the Human Glioblastoma Cell Culture (HGCC) resource (Uppsala University, Sweden). Cells were seeded onto poly-ornithine/laminin-coated plates and grown in Feed Medium [1:1 ratio of DMEM/F12 Glutamax (Gibco) and Neurobasal medium (Gibco), supplemented with 1X B27 (Gibco), 1X N-2 Supplement (Gibco), 1% penicillin/streptomycin (Gibco), 10 ng/ml EGF (Epithelial Growth Factor; PreproTech EC Ltd.) and 10 ng/ml FGF (Fibroblast Growth Factor; PeproTech EC Ltd)].

#### *Tumour spheres and brain spheroids*

3D tumour spheres were generated by culturing cells from the *EGFR* iCE5B + 6B, iPromoter and control

(∅) lines in 1.5% agarose-coated flasks at a density of $2–3 \times 10^6$ cells/flask for 8 days. Chick fetal brain spheroids were generated as previously described [19]. Briefly, brains were dissected from E12 embryos obtained from fertilized Bovan chicken eggs, and dissociated mechanically and enzymatically (accutase, 5 min). Isolated brain cells were seeded in 1.5% agarose-coated flasks ($10^6$ cells per $25cm^2$ flask) and grown in RPMI medium supplemented with 10% FBS (fetal bovine serum) and 1% penicillin/streptomycin (all from Gibco). 3D spheroid invasion assays were performed on 8-well chamber slides (Ibidi) by placing one tumour sphere and one brain spheroid per well, and either monitored with a EVOS M5000 imaging system over 24 h to assess fusion or imaged on a Leica widefield Thunder microscope at t = 96 h to determine invasion.

All cells were grown in a cell incubator at 37 °C in a humidified atmosphere (95% humidity) with 5% $CO_2$.

#### Luciferase dual-reporter assay

Luciferase assay was performed using the Promega Dual-Luciferase® Reporter Assay System following manufacturer's instructions. Conserved Elements (CE) were PCR-amplified from GB genomic DNA using GoTaq® G2 DNA Polymerase (Promega #M7845) (primer sequences listed in Supplementary Table S1) and cloned into pGL4.23[luc2/minP] vector (Promega Cat# E8411) using Acc65I and BglII restriction enzymes (Thermo Fisher). pGL4.23 + enhancer constructs were transfected into the U251 cells using Lipofectamine™ 2000 Transfection Reagent (Thermo Fisher) together with the pRL-SV40 vector (Promega Cat# E2231) for signal normalisation. pGL4.13[luc2/SV40] vector (Promega Cat# E6681) served as a positive control. Luminescence readings were taken using the Biotek Synergy HT microplate reader. Data was represented as fold change (FC) over empty pGL4.23 readings.

#### ChIP (Chromatin ImmunoPrecipitation)-qPCR

ChIP-qPCR was performed in stable glioblastoma lines established upon epigenomic perturbation of the *EGFR* enhancers, including the empty vector control lines, and in the parental U251 GB cell line. Briefly, cells were fixed on the plate by adding formaldehyde directly to the medium (final concentration 1% formaldehyde) for 15 min at room temperature while rotating. The crosslinking reaction was quenched by adding Glycine (final concentration 125 mM Glycine) for 5 min, and fixed cells were scraped off and harvested in 1X cold PBS containing protease inhibitors. Cells were then resuspended in lysis buffer ($3–6 \times 10^6$ cells/ml) and sonicated in a Covaris E220 instrument (shearing time 12 min, PIP 140, duty factor 5, 200 cycles per burst). Chromatin immunoprecipitation was performed with antibodies against H3K27ac (Abcam Cat# ab4729), H3K27me3 (Abcam Cat# ab192985) and H3K9me3 (Abcam Cat# ab8898) and using Dynabeads™ M-280 Sheep Anti-Rabbit IgG (Invitrogen Cat# 11203D). Chromatin Immunoprecipated DNA was amplified by qPCR using a CFX Connect Real-Time PCR Detection System (Bio-Rad) and primers specific for the genomic regions of interest (Supplementary Table S2). Positive and negative regions were measured in parallel for control purposes and enrichment was calculated over the input.

#### Generation of stable cell lines

##### *Cloning*

The UCSC genome browser (http://genome.ucsc.edu) tool 'CRISPR target identifier' was used to select CRISPR gRNAs. For CRISPRi, gRNAs targeting central regions of the CEs were cloned into the *pLV hU6-sgRNA hUbC-dCas9-KRAB-T2a-GFP* plasmid (Addgene_71237) using the BsmBI restriction sites (gRNA sequences listed in Supplementary Table S3). To generate genomic deletions, we modified this plasmid and cloned gRNAs targeting the flanks of the CEs. First, we replaced the dCas9-KRAB with an active Cas9 coding sequence, and further replaced GFP by mCherry, thus generating two new constructs hereby named *pLV hU6-sgRNA hUbC-Cas9-T2a-GFP* and *pLV hU6-sgRNA hUbC-Cas9-T2a-mCherry*. Deletion gRNAs were then cloned into these vectors. GFP and mCherry expression enabled subsequent FACS sorting of positively transduced cells.

##### *Lentivirus transduction*

Lentiviral particles were produced and collected upon transfection of HEK293T cells with the lentiviral Cas9 or dCas9 plasmids expressing the gRNAs, along with the psPAX2 (Addgene_12260) and pMD2.G (Addgene_12259) lentiviral packaging plasmids and using Lipofectamine™ 2000 (Thermo Fisher). Between 24–48 h post-transfection, the viral supernatant was filtered, supplemented with 20 mM HEPES and polybrene (10 µg/ml), and used for transduction of U251 or U3013 cells in three rounds.

##### *FACS sorting*

To establish stable lines, transduced cells were sorted by Fluorescence-Activated Cell Sorting (FACS) using the BD FACSAria™ III Cell Sorter instrument and the BD FACSDiva software. For CRISPRi experiments, GFP positive cells were collected and, in the case of CRISPR/Cas9-mediated genomic deletions double positive GFP + mCherry + cells were sorted and further expanded.

#### *Validation of cell lines*

Repression by CRISPRi was validated by measuring the enrichment of H3K9me3 by ChIP-qPCR (see methods section above). Genomic deletions were confirmed by genotyping PCR using primers designed to flank the gRNA target sequences. Genomic DNA (gDNA) was extracted using Qiagen DNeasy Blood & Tissue Kit (ID: 69504) and genotyping PCRs were performed using GoTaq® G2 DNA Polymerase (Promega #M7845) (genotyping primers are listed in Supplementary Table S4).

### RT-qPCR

Total RNA was extracted from cells using the RNeasy Plus Mini Kit (ID: 74,134, Qiagen). cDNA was synthesised using RevertAid H Minus Reverse Transcriptase (Thermo Fisher #EP0451) and random hexamers (Thermo Fisher #SO142), following the manufacturer's instructions. Quantitative-PCR analysis was performed with CFX Connect Real-Time PCR Detection System (Bio-Rad) using SYBR green master mix—PowerUp (Thermo Fisher). Gene expression levels were measured alongside the housekeeping gene *HPRT* for normalisation (qPCR primers listed in Supplementary Table S5). Relative expression levels were determined using the ΔΔCt method.

### Western blot

Whole cell protein extracts were prepared using lysis buffer containing 2% SDS and 0.1 M Tris–HCl pH 6.8. Protein concentration was measured using the Pierce™ BCA Protein Assay Kit (Thermo Scientific) and absorbance at 560 nm was determined using the Biosan HiPo MPP-96 microplate photometer. Protein samples were loaded into precast gels, run in the Mini-PROTEAN Tetra Cell and blotted using the Trans-Blot® Turbo™ Transfer System (all Bio-Rad) according to standard protocols. Primary antibodies against EGFR (1:1000, rabbit, Cell Signaling Cat# 4267) and GAPDH (1:1000, rabbit, Cell Signaling Cat# 2118) were diluted in 5% bovine serum albumin (BSA) in Tris-Buffered Saline 0.1% Tween® 20 Detergent. Peroxidase AffiniPure Goat Anti-Rabbit IgG (H + L) (1:10,000, Jackson ImmunoResearch Labs Cat# 111–035-003) was used for detection together with Bio-Rad Clarity Western ECL Substrate. ChemiDoc™ MP Imaging System with Image Lab™ Software (Bio-Rad) was used for signal detection and quantification.

### Live-cell imaging

All live-cell imaging experiments were performed using the IncuCyte S3 Live-Cell Analysis instrument (Sartorius) and the image analysis was performed using the Incucyte Base Analysis Software.

#### *Proliferation assays*

Cell proliferation was determined by live-cell imaging taking phase-contrast images every 4 h during a period of 72 h. Automated cell segmentation and counting was performed with the adherent Cell-by-Cell analysis software module. Data was normalised to the t = 0 h count and presented as ratios.

#### *Scratch wound assays*

Scratch wound assays were performed using the IncuCyte Wound Maker tool on cells seeded in ImageLock 96-well plates (Cat No 4379). Phase-contrast images were taken every 2 h and gap closure was determined as confluence measurements obtained with the automated Scratch Wound Analysis Software Module.

#### *Chemotactic migration assays*

Chemotactic migration was determined by imaging cells in the Incucyte® Clearview 96-Well Chemotaxis Plate (#4582), and analysed using the Chemotaxis Analysis Software Module. Cells were seeded in 1% FBS media in the trans-well insert and 10% FBS media was used as chemoattractant in the reservoir wells to stimulate migration of cells. A no-chemoattractant negative control was set up using 1% FBS in both the insert and reservoir wells.

#### *Annexin V apoptosis assays*

Incucyte® Annexin V Red Dye (Sartorius #4641) was added to the cell culture medium at a final dilution of 1:200 (as per product guidelines). Both phase-contrast and red fluorescence (Excitation: 567–607 nM, Emission 622–704 nM) images were taken every 4 h during a period of 72 h. A red area confluence mask was applied to the cells to measure the apoptotic cell area using the Incucyte Base Analysis Software. Data was expressed as red area confluence (%) and normalised to total cell count (red area/total phase area).

#### *Reactive oxygen species*

5 μM CellROX™ Deep Red Reagent (Invitrogen #C10422) was added to cells in culture. After 30 min of incubation time at 37 °C, the reagent was washed out twice with PBS and the cells were immediately imaged. Both phase-contrast and red fluorescence (Excitation: 567–607 nM, Emission 622–704 nM) images were taken. A mask was applied to the red fluorescent signal to measure integrated intensity (normalised to phase-contrast cell count).

#### *Temozolomide treatment*

U251 and U3013 cells were treated with 1 mM TMZ and 125 μM TMZ, respectively (Temozolomide, Sigma-Aldrich T2577, dissolved in DMSO (Dimethyl

Sulfoxide, Calbiochem—CAS 67–68-5). Cell proliferation was assessed in comparison to DMSO-treated control cells as above (see *Proliferation assays*). The TMZ concentrations used for each line were experimentally determined by serial titration, such as that the highest concentration not impacting the proliferation of the control (∅) lines was chosen.

#### Immunofluorescence

For immunofluorescence, cells were cultured as described above, fixed in 4% formaldehyde for 15 min at room temperature, permeabilized in 0.2% Triton-X100 for 5 min and subjected to incubation with an anti-cleaved caspase-3 antibody (Cell Signaling #9661). Images were taken using a Leica widefield Thunder microscope.

#### Measurement of mitochondrial function

Mitochondrial function was determined using the Seahorse XFe96 Analyzer (Agilent), which measures mitochondrial oxygen flux and extracellular acidification rate for live cells in real time. The Cell Mitochondrial Stress Test was performed following manufacturer's instructions and oxygen consumption rates (OCR) were determined. Seahorse 96 well-plates were coated with Poly-D-lysine (50 µg/ml, ThermoFisher Scientific, Cat# A3890401) and 20,000 cells were seeded per well. The test was performed as per standard protocol in XF assay medium (Dulbecco's Modified Eagle Medium (DMEM) + 5 mM glucose + 2 mM glutamine + 1 Mm pyruvate, pH7.4). 20 µM of oligomycin, 10 µM of FCCP and 5 µM rotenone + 5 µM Antimycin A were added to selectively inhibit different steps of mitochondrial respiration and thus initiate the relevant phases of the test. ATP production was calculated as (basal respiration – proton leak). Spare Respiratory Capacity (SRC) was determined as (maximal respiration – basal respiration).

#### Measurement of glutathione (GSH-to-GSSG) ratios

The GSH/GSSG-Glo™ Assay (Promega #V6611) was used to measure GSH/GSSG ratios and therefore infer oxidative stress levels (i.e., lower GSH/GSSG ratios are indicative of oxidative stress). 5,000 cells per well were seeded in white opaque 96-well plates and treated as per standard protocol. Luminescence readings were taken with the Biotek Synergy HT microplate reader using a 1 s integration time.

#### Statistical analysis

All statistical analysis was performed using GraphPad Prism software. Statistical tests, multiple comparison correction methods, number of replicates and significance are indicated in figure legends and in the corresponding figure panels. Figure legends also indicate the cases when the Welch's correction method was chosen to not assume equal SDs between groups.

## Results

#### Identification of novel *EGFR* enhancers in glioblastoma

We first identified a panel of 10 conserved elements (CE1-CE10) as potential candidates to regulate the expression of *EGFR* in glioblastoma. This identification was based on sequence conservation and *GeneHancer* prediction to interact with the *EGFR* promoter, together with our previous data on distribution of active chromatin marks and chromatin accessibility (Chakraborty et al. bioRxiv https://doi.org/10.1101/2022.11.16.516797.) (Fig. 1A). Two SNPs associated with increased GB risk are located in the *EGFR* locus: rs723527, within intron 1, and rs75061358, ~ 150 kb upstream of the *EGFR* transcription start site (TSS) [20]. Of these, rs723527 is located within one of these conserved elements (CE5), in a highly accessible region and enriched in the active enhancer mark H3K27ac in a panel of patient-derived

(See figure on next page.)

**Fig. 1** Identification of novel *EGFR* enhancers in glioblastoma located in the vicinity of the GB-associated SNP rs723527. **A**, Schematic representation of the *EGFR* gene locus displaying: GB-associated SNPs; *GeneHancer* predicted interactions between genomic regions and the *EGFR* promoter; H3K27ac enrichment in seven ENCODE cell lines; H3K27ac enrichment and chromatin accessibility by ATAC-seq across three representative patient-derived GB cell lines (our previous data Chakraborty et al. bioRxiv doi.org/10.1101/2022.11.16.516797); and the conserved elements (CE) selected for characterisation highlighted in grey. Visualisation in the UCSC genome browser. **B**, Enrichment of H3K27ac and H3K27me3 in U251 glioblastoma cells around the CE regions as determined by ChIP-qPCR. **C**, Enhancer dual-luciferase reporter assay. Luciferase activity relative to the control reporter plasmid is expressed as a fold change. Data is presented as mean ± SEM ($n = 5$). **D**, Schematic representation of the deletion and repression CRISPR-perturbation strategies. **E**, Enrichment of H3K9me3 upon expression of the transcriptional repressor KRAB in the CRISPRi-repressed U251 cell lines as determined by ChIP-qPCR. **F**, *EGFR* gene expression relative to *HPRT* in each KRAB-repressed U251 line (i.e. iCEx) as determined by RT-qPCR. Data is represented as mean ± SEM ($n = 4$). Statistical significance was assessed by unpaired *t* test with Welch's correction (** $P < 0.01$). **G**, Cropped results from western blot, displaying EGFR and GAPDH protein expression (full uncropped blots in Supplementary Fig. 6)

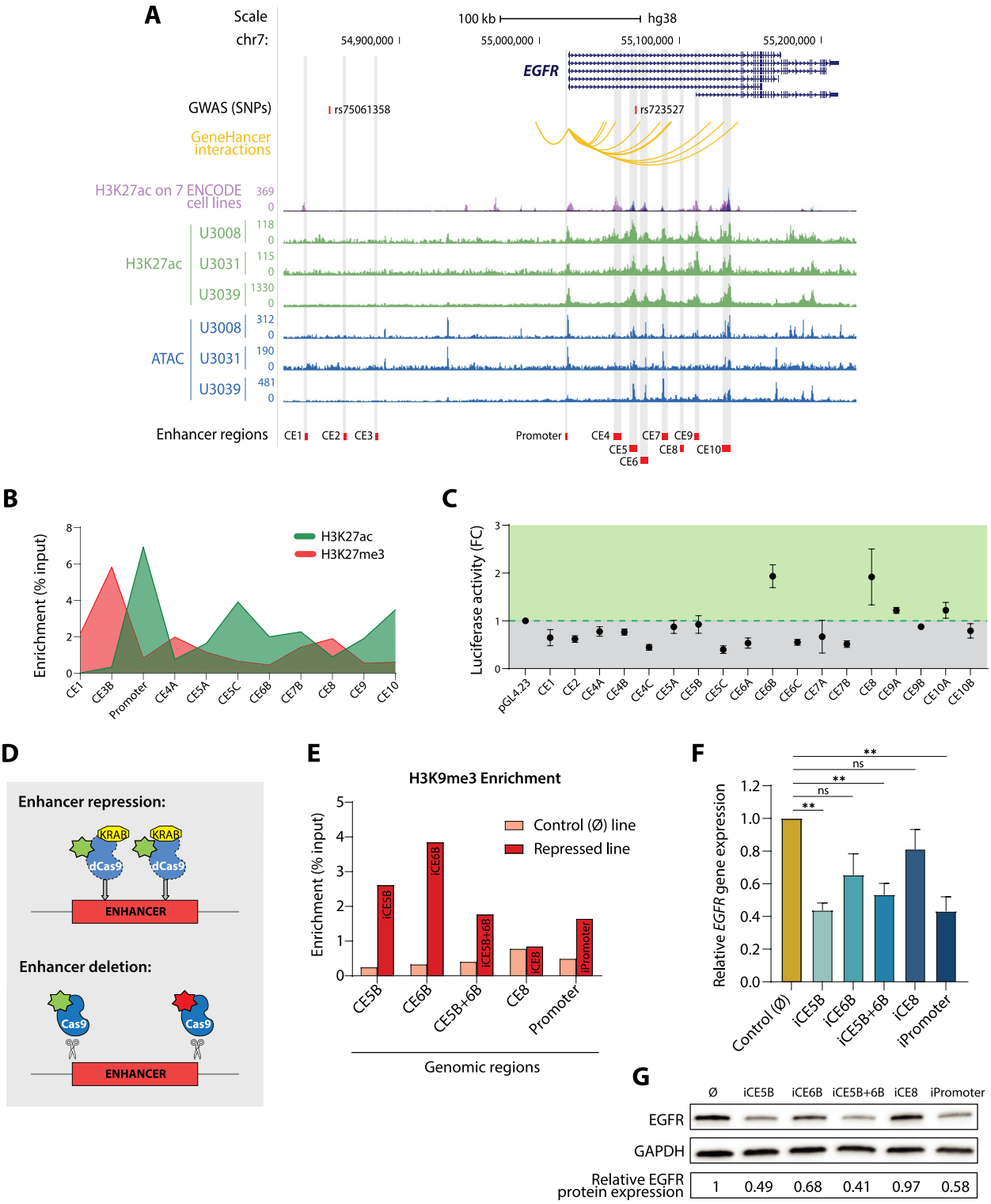


**Fig. 1** (See legend on previous page.)

glioblastoma cell lines (Fig. 1A and Chakraborty et al. bioRxiv https://doi.org/10.1101/2022.11.16.516797.). In contrast, rs75061358 is not located within one of the CEs and does not display any features indicative of enhancer activity. We made similar observations regarding the distribution of chromatin marks around these SNPs in U251

glioblastoma cells, as measured by ChIP-qPCR (Fig. 1B). In particular subregions CE5C and CE6B, which are proximal to the SNP rs723527, displayed enrichment of the active enhancer mark H3K27ac and depletion of the repressive mark H3K27me3.

To determine the regulatory potential of these 10 conserved elements (CEs), we employed luciferase reporter assays in U251 cells. For large CEs (>2 kb), smaller regions were subcloned and tested (e.g. CE5 A, B and C regions). CE6B and CE8 retained the highest regulatory potential on enhancer reporter assays (Fig. 1C), where CE6B is located closest to the GB-associated SNP rs723527. In contrast, CEs located close to rs75061358 did not demonstrate enhancer activity in these reporter assays. These findings therefore highlight three putative enhancer elements: CE5, CE6 and CE8, which are located within intron 1 of *EGFR* and in close proximity to rs723527.

#### CRISPR-perturbation of novel *EGFR* enhancers decreases *EGFR* gene expression and protein levels

To functionally demonstrate that the identified CEs act as *EGFR* enhancers in glioblastoma, we introduced targeted perturbations utilising both CRISPRi (dCas9-KRAB) and CRISPR/Cas9. We generated various U251 glioblastoma cell lines with either stable epigenomic repression of the CEs or carrying the deletions of interest (Fig. 1D) and validated our key findings in an independent GB cell line, U3013, more recently established by the HGCC (the Human Glioblastoma Cell Culture). As expected, upon recruitment of the transcriptional repressor KRAB to the CEs, the established lines showed an enrichment of the repressive mark H3K9me3 in the corresponding region, in comparison to the empty vector control line (Fig. 1E, Supplementary Fig. S1A-F). dCas9-KRAB repression of the CEs (hereby iCE) correlated with significant downregulation of *EGFR* gene expression in both U251 and U3013 cell lines (Fig. 1F, Supplementary Fig. S2A), and lower protein levels (Fig. 1G). For iCE5B, iCE5B + 6B and the iPromoter region, *EGFR* gene expression levels were significantly reduced to 44%, 53% and 43% of the expression observed in the control line, respectively (Fig. 1F). Similarly, protein levels were reduced to 49%, 41% and 58% of the control line levels (Fig. 1G). Only in the case of iCE8, the level of repression indicated by enrichment of H3K9me3 was not sufficient to considerably diminish the EGFR protein levels. Furthermore, the cell lines carrying genomic deletions (Supplementary Fig. S3A) also present a significant downregulation of *EGFR* gene expression accompanied by reduced protein levels (Supplementary Fig. S3B, C). In the ΔCE5B + 6B, ΔCE6B, ΔCE8 and ΔPromoter lines, *EGFR* expression is reduced to 29%, 48%, 66% and 70% of the control line levels, respectively (Supplementary Fig. S3B). Therefore, CRISPR-based perturbation of the CEs with regulatory potential demonstrates, in a functional manner, that they act as *EGFR* enhancers in the context of glioblastoma.

#### Repressing the *EGFR* enhancers reduces the proliferative and invasive capacity of glioblastoma cells

Having determined the impact of enhancer perturbation on *EGFR* expression, we then evaluated the proliferative and invasive capacities of the enhancer-perturbed glioblastoma lines. Firstly, we assessed cell proliferation by live-cell imaging using the IncuCyte S3 live-cell analysis instrument and automated cell counting software. Cell lines with independent repression of CE5B and CE6B displayed a modest reduction in their proliferative capacity in comparison to the control (Fig. 2A). However, CRISPRi of the large region comprising CE5B + 6B, which includes the SNP rs723527, significantly reduced the cell proliferation of glioblastoma cells to almost the same extent as the *EGFR* promoter-repressed cell line (Fig. 2A, B). The same effect was observed in the U3013 iCE5B + 6B cell line (Supplementary Fig. S2B). CRISPR/Cas9-mediated deletion of the *EGFR* enhancers demonstrated slight inhibition of proliferation, though statistically insignificant, in all cell lines carrying the enhancer deletions (Supplementary Fig. S3D). The proliferative defect observed in the enhancer-repressed cell lines is much stronger than that of the enhancer-deletion lines, likely due to the spreading of the repressive marks over a larger region. Together with the added advantage that CRISPRi with dCas9-KRAB does not involve direct modification of the DNA sequence but solely epigenomic editing, we focused our further investigation on the *EGFR* enhancer-repressed glioblastoma cell lines.

Next, we assessed the invasive capacity of the *EGFR* enhancer-repressed lines through different approaches. In scratch wound healing assays, we observed that the iCE5B + 6B and iPromoter cells were migrating towards the gap at a significantly lower rate than the control (∅) U251 cells (Fig. 2C, D). This data shows that epigenomic repression of the *EGFR* CE5B + 6B enhancer and promoter results in a decreased migrative capacity. We also observed that *EGFR* enhancer-repressed tumour spheres tend to display a reduced fusion and invasion capacity, when confronted with chick brain spheroids in 3D spheroid invasion assays (Supplementary Fig. S4A-D). In addition, we determined the invasive capacity of the *EGFR* enhancer-repressed lines by measuring their migration rate towards a chemical stimulus in chemotaxis migration assays. In these trans-well chemotactic assays, cells migrate through cell-permeable pores attracted by higher concentration of nutrients (i.e., from

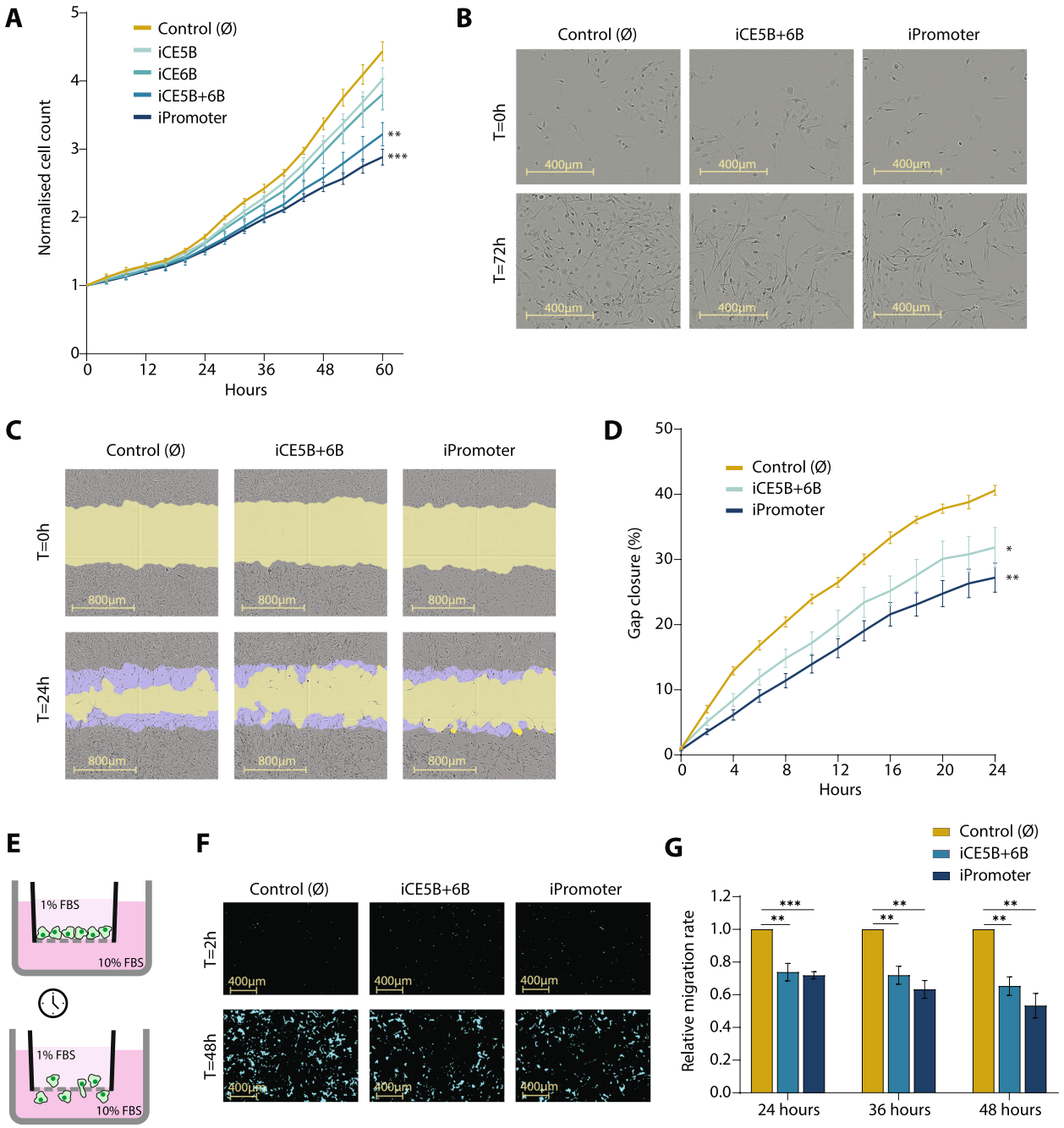


**Fig. 2** CRISPRi of novel *EGFR* enhancers reduces the proliferation and migration of U251 glioblastoma cells. **A**, Proliferation rates of the *EGFR* enhancer-repressed lines determined by live-cell imaging. Images were acquired every 4 h and proliferation was determined by automatic cell count. Data is normalised to t = 0 and presented as mean ± SEM ($n = 4$). Statistical significance was assessed by unpaired *t* test with Welch's correction (** $P < 0.01$, *** $P < 0.001$). **B**, Representative images of control cells alongside iCE5B + 6B and iPromoter cell lines at t = 0 h and t = 72 h. **C**, Images showing gap closure rate of control, iCE5B + 6B and iPromoter cells at 0 h and 24 h. Yellow area represents the gap area at each time point, and blue area highlights the migration area. **D** Gap closure rate (%) between 0 and 24 h. Data is presented as mean ± SEM ($n = 5$). Statistical significance was assessed by unpaired *t* test with Welch's correction (* $P < 0.05$, ** $P < 0.01$). **E**, Schematic representation of the chemotactic migration assay. **F**, Representative images from the chemotactic assays taken at t = 2 h and t = 48 h. Masked area (blue) covers cells that migrated through the pores of the culture plate towards the chemoattractant. **G** Relative migration rates of iCE5B + 6B and iPromoter cell lines represented as total masked area of migrated cells at t = 24 h, t = 36 h and t = 48 h, normalised to the initial seeding density. Data is presented as mean ± SEM ($n = 3$). *P* values were determined by unpaired *t* test (** $P < 0.01$, *** $P < 0.001$)

1 to 10% FBS) and are monitored in real-time (Fig. 2E). As a negative control, a no-chemoattractant condition was established (i.e., 1% to 1% FBS) (Supplementary Fig. S4E-G). We observed that the migrative capacity of the iCE5B + 6B cell line was significantly compromised (Fig. 2F-G), similar to that observed upon repression of the *EGFR* promoter. Altogether, these findings show that repressing the *EGFR* enhancer region CE5B + 6B, which encompasses the GB-associated SNP rs723527, leads to significantly decreased proliferation, migration and invasion of glioblastoma cells.

### Reduced malignancy of the *EGFR*-enhancer repressed GB cells can be linked to increased apoptosis and mitochondrial respiration

We further characterised the *EGFR*-enhancer repressed lines by firstly measuring their relative apoptosis rates over time by live-cell imaging of cell cultures in the presence of annexin V red dye. The apoptotic cells (i.e., annexin V positive area) in the iCE5B + 6B repressed GB line increased at a significantly faster rate compared to the control cell line (Fig. 3A, D). The rate of apoptosis within the individually repressed CE5B and CE6B cell lines does not significantly differ from the unmodified control cells, and interestingly, nor does the promoter-repressed cell line. This effect is also observed when we account for differences in proliferation rate by normalising the annexin V-positive area to the total cell population area. We observed that after 48 and 72 h in culture, the percentage of annexin V-positive area in the iCE5B + 6B cell line is significantly higher than that of the control line (Fig. 3B, C). In line with this, the iCE5B + 6B cells also display a higher percentage of cleaved caspase-3 positive cells than the control line (Fig. 3E). This altogether suggests that targeting the CE5B + 6B enhancer region specifically causes an apoptotic response which cannot be triggered by repressing the promoter of *EGFR*.

Cancer cell metabolism is a key factor contributing to the cells' ability to evade apoptosis. In order to examine whether this increased rate of apoptosis observed in the iCE5B + 6B GB line was linked to changes in cellular metabolism, we performed a Seahorse Cell Mito Stress Test (Fig. 3F, G) to measure the relative oxygen consumption rates (OCR) of the cell lines as an assessment of mitochondrial function. We found that the iCE5B + 6B-repressed line presents a significantly higher basal and maximal OCR compared to the control line (Fig. 3H). This would suggest that these *EGFR*-enhancer repressed cells are favouring mitochondrial respiration over glycolysis. Based on the same assay, we can also extract that the ATP production and spare respiratory capacity (SRC) of the enhancer-repressed line increased significantly over the control (Fig. 3I, J). Moreover, the increased mitochondrial respiratory parameters in the iCE5B + 6B cell line are accompanied by significantly increased production of ROS (Reactive Oxygen Species) (Fig. 3K) and reduced ratio of reduced glutathione (GSH) to oxidised glutathione (GSSG) (i.e. GSH/GSSG) (Fig. 3L), both indicative of increased oxidative stress. We also observed alterations in the expression of several key metabolic genes, including those encoding for lactate dehydrogenase; the TCA cycle enzymes fumarase and malate dehydrogenase, and some subunits of the electron transport chain (ETC) (Supplementary Fig. S5). These findings indicate that epigenomic perturbation of the CE5B + 6B enhancer region causes increased mitochondrial respiration, resulting in an increased production of ROS, which would contribute to the apoptotic response observed.

### Epigenomic perturbation of the *EGFR* enhancers sensitises glioblastoma cells to TMZ treatment

Since temozolomide (TMZ) is the first-choice chemotherapeutic agent to treat GB clinically, we wanted

(See figure on next page.)

**Fig. 3** Epigenomic perturbation of the *EGFR* enhancer CE5B + 6B in U251 cells triggers apoptosis and favours mitochondrial respiration. **A**, Apoptosis levels in the *EGFR* enhancer-repressed lines as determined by annexin V red fluorescence area (% confluence) measured at 4-h intervals. Data is presented as mean ± SEM ($n = 3$). *P* values were determined by unpaired *t* test with Welch's correction (* $P < 0.05$). **B**-**C**, Apoptosis rate represented as proportion of the area occupied by annexin V red apoptotic cells *vs* total cells at t = 48 h (**B**) and t = 72 h (**C**). Data is presented as mean ± SEM ($n = 3$). Statistical significance was determined by unpaired *t* test (* $P < 0.05$, ** $P < 0.01$). **D**, Representative phase-contrast images of control cells and iCE5B + 6B cells alongside annexin V-positive cells (red) to identify apoptotic cells at t = 0 h and t = 72 h. **E**, Percent of cleaved caspase-3 positive cells, determined by immunofluorescence, after 48 h culture time in 1% FBS. Data is plotted as mean ± SEM ($n = 6$, > 100 cells per image). *P* values were determined by unpaired *t* test (**** $P < 0.0001$). **F**, Schematic representation of the Agilent Seahorse XF Cell Mito Stress Test. **G**, Oxygen Consumption Rate (OCR) of control cells and iCE5B + 6B enhancer-repressed cells in response to the assay compounds. Data is plotted as mean ± SEM ($n = 3$). **H**-**J**, Basal and maximal respiration (**H**), ATP production (**I**) and spare respiratory capacity (**J**) of control cells and iCE5B + 6B enhancer-repressed cells as determined by Cell Mito Stress Test. *P* values were determined by unpaired *t* test (** $P < 0.01$, **** $P < 0.0001$). **K**, Levels of reactive oxygen species (ROS) in control and iCE5B + 6B cells represented as integrated red fluorescent intensity per cell count. Data is presented as mean ± SEM ($n = 3$). Statistical significance assessed by unpaired *t* test with Welch's correction (* $P < 0.05$). **L,** Oxidative stress, determined by the ratio of reduced (GSH) and oxidised glutathione (GSSG). Data is presented as mean ± SEM ($n = 3$). *P* values were determined by unpaired *t* test (* $P < 0.05$)

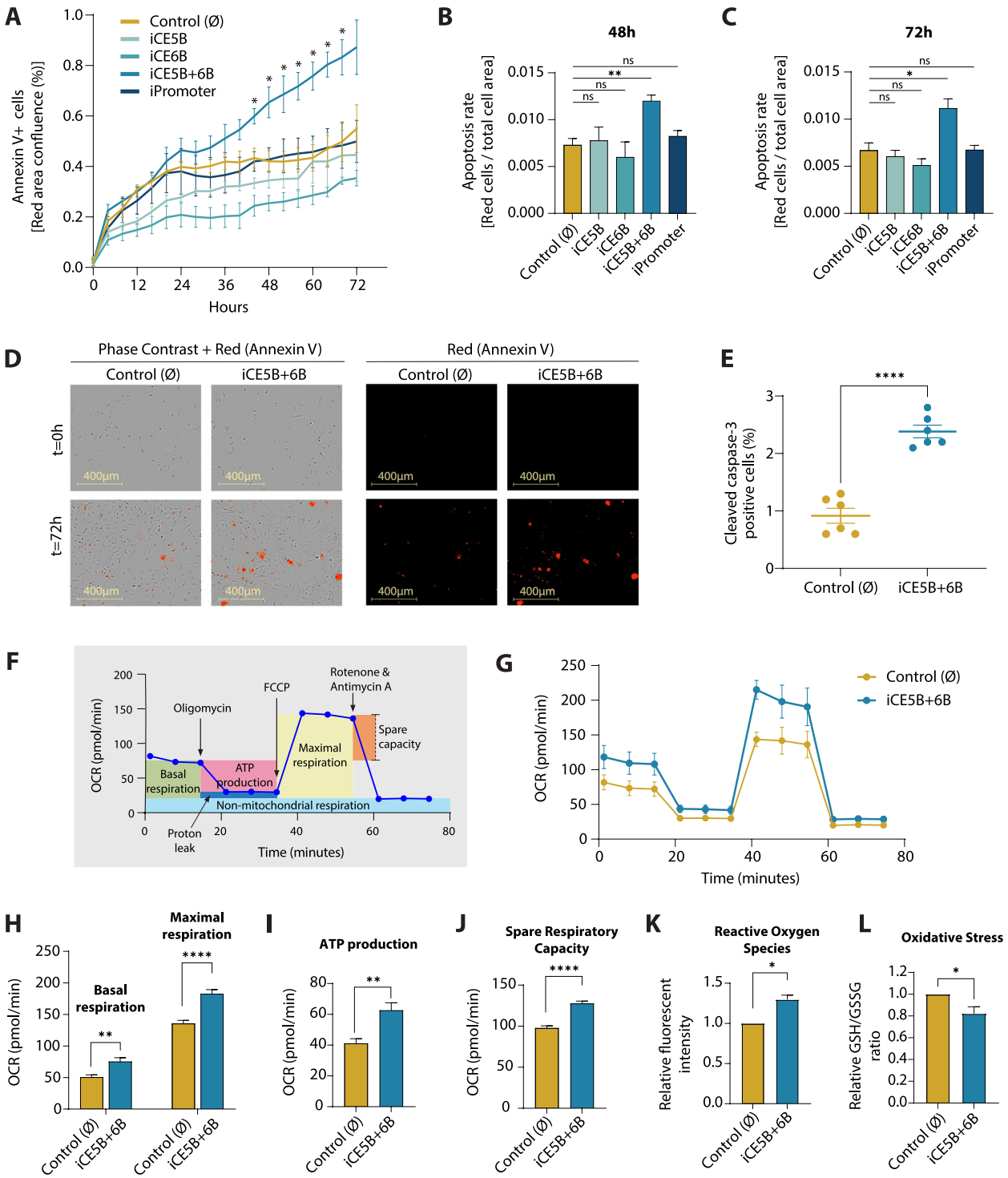


**Fig. 3** (See legend on previous page.)

to address how the *EGFR*-enhancer repressed lines respond to treatment with the drug. Not only the combined iCE5B+6B, but also the individual iCE5B, iCE6B and the *EGFR* iPromoter lines, showed a significantly slower proliferation rate upon TMZ treatment than the DMSO-treated controls (Fig. 4B-E and F). On the contrary, the empty vector control line is not significantly affected by TMZ treatment at the used concentration

(Fig. 4A, F). These findings were also corroborated independently in U3013 GB cells. While the control U3013 cells were not affected by TMZ treatment, the proliferation of iCE5B + 6B enhancer-repressed cells was reduced by TMZ at the given dose (Supplementary Fig. S2C-D). Moreover, TMZ treatment increases the percentage of cleaved caspase-3 positive cell ~ 1.8 times over the DMSO-treated conditions in the control (∅) line (Fig. 4G, H). However, in the iCE5B + 6B line, TMZ raises the levels of apoptosis cells ~ 3.3 times over the DMSO-treated condition (Fig. 4 G, H). Therefore, epigenomic repression of *EGFR* regulatory elements (i.e., novel enhancers and promoter), and subsequent downregulation of *EGFR* gene expression, sensitises glioblastoma cells to TMZ treatment. Our results show that combining epigenomic perturbation of enhancers or gene promoters with existing cancer drugs could improve the effectiveness of current treatments and subsequently the prognosis of patients.

## Discussion

This study identified novel enhancers that drive the expression of *EGFR* in glioblastoma cells. CRISPR-mediated (epi-)genomic perturbation (i.e., repression, deletion) of these enhancer regions has a direct effect on the survivability and invasiveness of glioblastoma cells. By specifically repressing the CE5B + 6B enhancer region that encompasses the known GB-associated SNP rs723527, we can lower *EGFR* expression levels and modulate the aggressiveness of glioblastoma cells, which become less proliferative and invasive.

One underlying component of this is an apparent shift in the cellular metabolism upon enhancer perturbation and subsequent *EGFR* downregulation. The *EGFR* iCE5B + 6B cells increase their basal and maximal mitochondrial respiratory activity, indicating a shift from the typical preference for glycolysis that is a common hallmark of cancerous cells [21–23]. Higher mitochondrial respiration rates result in greater production of reactive oxygen species (ROS), which in turn can inhibit cell growth, damage cellular components and induce cell death [24, 25]. Deregulation of ROS production and ROS limitation pathways are common features of cancer cells [26]. The metabolic rewiring in favour of mitochondrial respiration that we observe in the *EGFR* iCE5B + 6B cells is accompanied by an increased accumulation of ROS and, subsequently, an increase in apoptotic events. This ultimately contributes to a reduction of cell proliferation upon repression of the *EGFR* enhancers in glioblastoma.

In addition, there is a known bidirectional crosstalk between metabolism and epigenetics such that they reciprocally modulate each other in cancer [27, 28]. Therefore, one could speculate that the epigenomic perturbations that we introduced in the *EGFR* enhancer could underlie the observed metabolic switch through a mechanism to be determined. Recent reports have pointed the relevance of different metabolic pathways in GB, as drivers of chemoresistance [29] or by promoting immunosuppression during tumour evolution [30]. Besides, modulating energy metabolism to achieve antitumoral effects is emerging as a potential therapy for GB patients [31].

Migration of cancer cells in response to chemical stimuli is an important mechanism in the tumour dissemination process, both locally and during metastatic progression [32]. The tumour-associated microglia and macrophages (TAMs) present in the GB tumour microenvironment release growth factors and cytokines, including EGF (Epidermal Growth Factor) and CSF-1, which can promote tumour proliferation, survival and invasion [33, 34]. Our *EGFR* enhancer-repressed glioblastoma cells also present a reduced response to chemo-attractive stimuli and express less *EGFR* than the parental unmodified cells. One could therefore speculate that in vivo they might be less responsive to EGF being secreted by macrophages in the tumour microenvironment and could therefore be less invasive.

Repressing the CE5B + 6B *EGFR* enhancer reduces the proliferative and invasive capacity of GB cells, therefore ameliorating the malignant phenotype of glioblastoma cells, while additionally sensitising the cells to temozolomide: the current chemotherapeutic of choice in the clinic. The nature of the relationship between *EGFR* amplification levels and the response to TMZ treatment remains inconclusive and under debate [35]. In our study, upon enhancer repression,

(See figure on next page.)

**Fig. 4** Epigenomic repression of the novel *EGFR* enhancers sensitises U251 cells to temozolomide (TMZ) treatment. **A**-**E**, Proliferation rates of the *EGFR* enhancer-repressed lines determined by live-cell imaging upon treatment with 1 mM TMZ in comparison with the DMSO-treated control. Images were acquired every 4 h and proliferation was determined by automatic cell count. Data is normalized to t = 0 h and represented as mean ± SEM ($n = 3$). *P* values were determined by unpaired *t* test (* $P < 0.05$, ** $P < 0.01$). **F**, Representative images of control, iCE5B, iCE6B, iCE5B + 6B and iPromoter cells upon TMZ treatment in comparison to DMSO-treated controls at t = 72 h. **G**, Percent of cleaved caspase-3 positive cells, determined by immunofluorescence, after 48 h treatment with TMZ (1 mM) *vs* DMSO. Data is plotted as mean ± SEM ($n = 6$). *P* values were determined by unpaired *t* test (*** $P < 0.001$, **** $P < 0.0001$). **H**, Representative images of cleaved caspase-3 positive apoptotic cells in the iCE5B + 6B line following 48 h treatment with TMZ (1 mM). Scale bars 50 µm

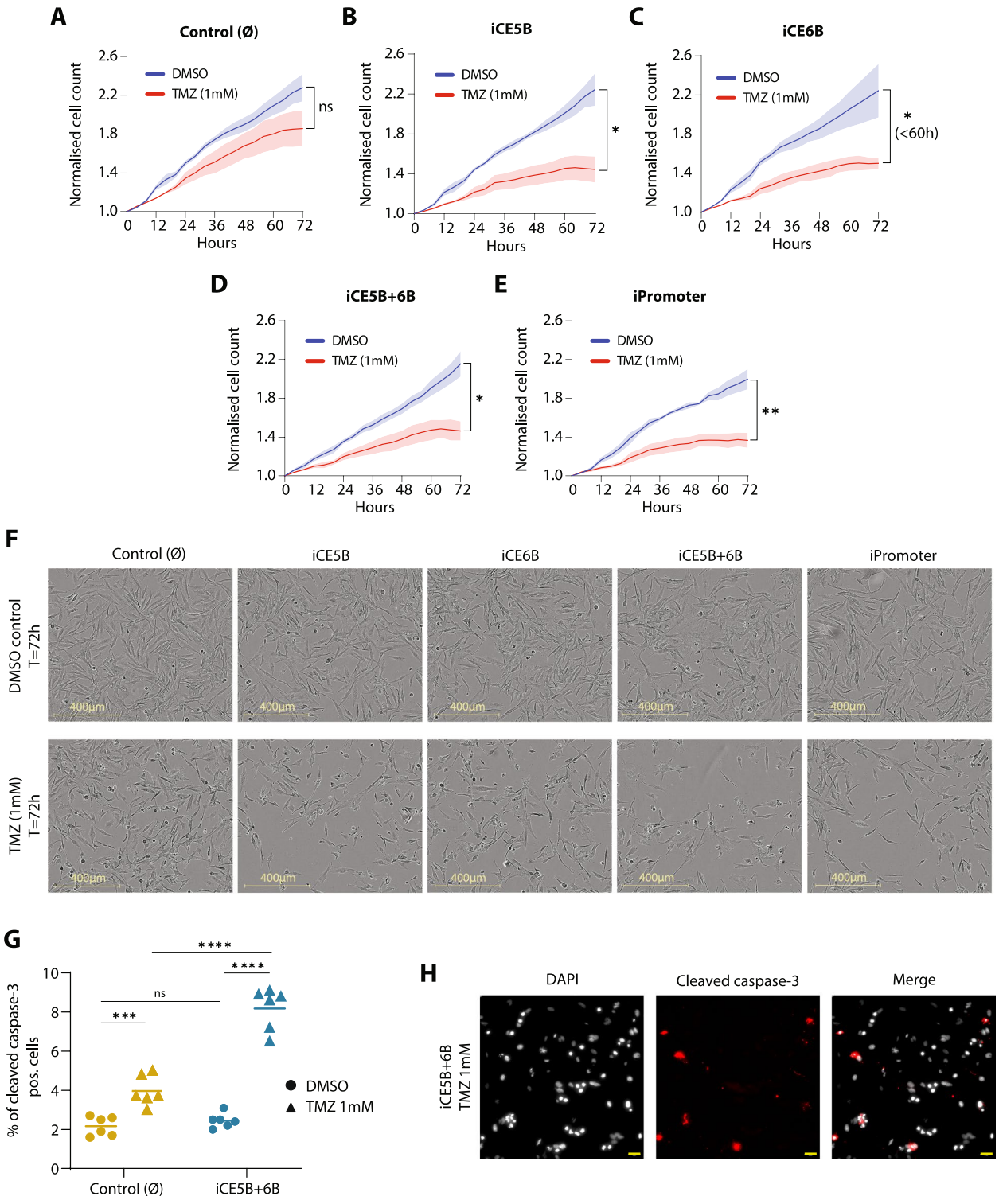


**Fig. 4** (See legend on previous page.)

lower *EGFR* levels correlate with an improved response to TMZ, at least in part due to an enhanced apoptotic response. Our findings point to an increased effect of temozolomide in combination with *EGFR* enhancer perturbation that may provide an effective combination therapy.

While EGFR as a therapeutic target has so far proven clinically unsuccessful in GB [36], lessons should be

learnt through the limitations of previous trials. Poor blood brain barrier (BBB) penetrance of drugs, a lack of patient stratification based on *EGFR* mutation status, studies performed primarily in the recurrent disease setting, and a lack of sustained EGFR inhibition have all contributed to a poor therapeutic response [37]. In light of this, EGFR should not be neglected as a potential therapeutic target in GB and our findings can help to open up new therapeutic possibilities.

Taken together, our data highlights the functional importance of the *EGFR* regulatory genome in glioblastoma and it demonstrates the potential of enhancer modulation as a therapeutic strategy. In the future, the combination of epigenomic perturbation of enhancers and current anti-cancer drugs can improve their effectiveness and subsequently the prognosis of difficult-to-treat cancers, such as glioblastoma.

## Supplementary Information

The online version contains supplementary material available at https://doi.org/10.1186/s12885-023-11418-9.

**Additional file 1: Supplementary Figure 1.** Recruitment of dCas9-KRAB repressor complex leads to enrichment of H3K9me3 at specic targeted sites in U251 cells. A-F, Bar charts depicting the enrichment of H3K9me3, as determined by ChIP-qPCR, at each genomic region (i.e., CE5B, CE6B, CE8, Promoter) and in each of the *EGFR* enhancer-repressed lines: iCE5B (B), iCE6B (C), iCE5B+6B (D) and iCE8 (E), alongside the iPromoter (F) and control line (A). **Supplementary Figure 2.** CRISPRi of *EGFR* enhancer CE5B+6B in Human Glioblastoma cell line U3013 downregulates *EGFR* gene expression, reduces cell proliferation rate, and sensitises cells to temozolomide (TMZ). A, *EGFR* gene expression as determined by RT-qPCR. B, Proliferation rates of the iCE5B+6B and promoter-repressed U3013 cell lines determined by live-cell imaging. Images were acquired every 4 hours and proliferation was determined by automatic cell count. Data is normalised to t=0 and presented as mean ± SEM ($n$=3). Statistical significance was assessed by unpaired $t$ test (* $P < 0.05$, ** $P < 0.01$). C-D, Proliferation rates of control U3013 and iCE5B+6B enhancer-repressed U3013 cells determined by live-cell imaging upon treatment with 125μM TMZ in comparison with the DMSO-treated control. Images were acquired every 4 hours and proliferation was determined by automatic cell count. Data is normalised to t=0h and represented as mean ± SEM ($n$=4). $P$ values were determined by unpaired t test. **Supplementary Figure 3.** CRISPR/Cas9-mediated deletion of *EGFR* enhancers in U251 cells downregulates *EGFR* gene expression and affects cell proliferation rates. A, Genotyping PCR of the *EGFR* enhancer-deleted cell lines (ΔCE5B, ΔCE6B, ΔCE5B+6B, ΔCE8) alongside the Δ Promoter and empty vector control lines (left), and schematic outline of the PCR genotyping strategy (right). Note that the wild-type CE5B+6B allele is too large to be amplied under these conditions. Full uncropped gel image presented in Supplementary Figure 6. B, *EGFR* gene expression levels relative to *HPRT* in *EGFR* enhancer-deleted cell lines as determined by RT-qPCR assays. Data is represented as mean ± SEM ($n$=3). Statistical significance as assessed by unpaired $t$ test with Welch's correction (* $P < 0.05$, ** $P < 0.01$). C, Cropped western blots showing EGFR protein expression and normalised to GAPDH protein levels (full uncropped blots in Supplementary Figure 6). D, Proliferation rates of cell lines carrying *EGFR* enhancer deletions or promoter deletions as determined by live-cell imaging, and in comparison to the empty vector control line. Images were acquired every 4 hours and proliferation was determined by automatic cell count. Data is normalised to t= 0h and plotted as mean ± SEM ($n$=3). **Supplementary Figure 4.** CRISPRi of the *EGFR* enhancer CE5B+6B and promoter compromises the invasive capacity of U251 cells. A, Representative images of the fusion between the fetal brain spheroids and the GFP+ tumour spheres generated from control, iCE5B+6B and iPromoter lines. Scale bars 750μm (0h) and 300μm (2-24h). B, Quantication of fusion events across a pool of independent tumour sphere/brain spheroid confrontation assays ($n$=10). C, Quantication of invasion frequency between the GFP+ tumour spheres and brain spheroids between 0h and 96h. D, Representative images of invasion/non-invasion between GFP+ tumour spheres and brain spheroids. Scale bar 100μm. Arrowheads point to areas of invasion. E-F, Line plots comparing the rate at which the respective cell lines migrate either from media containing 1% FBS to 1% FBS (no-chemoattractant negative control) or from 1% FBS to 10% FBS (chemoattractant condition). Migration was assessed by live-cell imaging taking images every hour and migration rate was determined by automatic quantification of the area of migrated cells. Data is represented as mean ± SEM ($n$=3). **Supplementary Figure 5.** Expression of key metabolic genes in the *EGFR* enhancer-repressed iCE5B+6B cell line. A, Results from qPCR analysis where certain metabolic genes are upregulated in the iCE5B+6B line relative to the control. Gene expression levels are relative to *HPRT*. **Supplementary Figure 6.** Uncropped western blot and gel images. A-B, Western blot on repressed cell lines (A) and deletion cell lines (B) detecting EGFR and GAPDH expression. Cropped images presented in Figure 1G and Supplementary Figure 3C, respectively. C, Uncropped genotyping gel from enhancer-deletion U251 cell lines. Cropped image presented in Supplementary Figure 3A.

#### Acknowledgements
We acknowledge the Biochemical Imaging Center at Umeå University and the National Microscopy Infrastructure, NMI (VR-RFI 2019-00217) for providing assistance in microscopy, and the Umeå University Flow Cytometry platform for assistance with cell sorting. Seahorse analyses were performed at the Seahorse Platform, Umeå University. We also thank Helena Edlund for providing the pSPAX and pMD2.G plasmids and GAPDH antibody; Lena Gunhaga for the fertilized eggs; and Ulf Ahlgren for the cleaved caspase-3 antibody.

#### Authors' contributions
CA-V designed, performed, analysed and interpreted most of the experiments and wrote the original manuscript draft. IN performed ChIP-qPCR experiments, and contributed to qPCR analysis and image acquisition. SD performed the 3D spheroid assay. AH contributed to data interpretation and manuscript editing. SR designed and supervised the study, secured funding, analysed and interpreted the data, and wrote and edited the final manuscript with input from the other authors.

#### Funding
Open access funding provided by Umea University. Research in SR's laboratory is supported by the Swedish Research Council (2019–01960), the Swedish Cancer Foundation (21 1720), Knut och Alice Wallenbergs Stiftelse (WCMM, Umeå), the Kempe Foundation (SMK-1964.2), as well as the Cancer Research (AMP 19–977, AMP 22–1091, AMP 23–1137) and Lion's Cancer Research Foundations in Northern Sweden (LP 21–2290).

#### Availability of data and materials
Data depicted on Fig. 1A is available: a) via the UCSC browser for the tracks displaying the GeneHancer interactions and H3K27ac on 7 ENCODE cell lines, or b) retrieved from GEO (Gene Expression Omnibus) with the accession number GSE217349 for the tracks displaying H3K27ac and ATAC in the glioblastoma lines U3008, U3031 and U3039. Other materials can be available from the corresponding author, SR, upon reasonable request.

## Declarations

#### Ethics approval and consent to participate
Not applicable.

#### Consent for publication
Not applicable.

#### Competing interests
The authors declare no competing interests.

Received: 23 March 2023 Accepted: 18 September 2023
Published online: 06 October 2023

## References


1. Poon MTC, Sudlow CLM, Figueroa JD, Brennan PM. Longer-term (≥ 2 years) survival in patients with glioblastoma in population-based studies pre- and post-2005: a systematic review and meta-analysis. Sci Rep-uk. 2020;10:11622.
2. Stewart BW, Wild CP. World Cancer Report 2014. International agency for research on cancer, WHO (World Health Organization). 2014. ISBN 978-92-832-0443-5.
3. Young RM, Jamshidi A, Davis G, Sherman JH. Current trends in the surgical management and treatment of adult glioblastoma. Ann Transl Medicine. 2015;3:121.
4. Stupp R, Taillibert S, Kanner A, Read W, Steinberg DM, Lhermitte B, et al. Effect of tumor-treating fields plus maintenance Temozolomide vs maintenance Temozolomide alone on survival in patients with glioblastoma: a randomized clinical trial. JAMA. 2017;318:2306–16.
5. Stupp R, Taillibert S, Kanner AA, Kesari S, Steinberg DM, Toms SA, et al. Maintenance therapy with tumor-treating fields plus Temozolomide vs Temozolomide alone for glioblastoma: a randomized clinical trial. JAMA. 2015;314:2535–43.
6. The National Institute for Health and Care Excellence. Brain tumours (primary) and brain metastases in adults NICE guideline [NG99]. 2018. https://www.nice.org.uk/guidance/ng99.
7. Rominiyi O, Vanderlinden A, Clenton SJ, Bridgewater C, Al-Tamimi Y, Collis SJ. Tumour treating fields therapy for glioblastoma: current advances and future directions. Br J Cancer. 2021;124:697–709.
8. Guzauskas GF, Pollom EL, Stieber VW, Wang BCM Jr, LPG. Tumor treating fields and maintenance temozolomide for newly-diagnosed glioblastoma: a cost-effectiveness study. J Méd Econ. 2019;22:1006–13.
9. Hegi ME, Diserens AC, Gorlia T, Hamou MF, de Tribolet N, Weller M, et al. MGMT gene silencing and benefit from temozolomide in glioblastoma. New Engl J Med. 2005;352:997–1003.
10. Alnahhas I, Alsawas M, Rayi A, Palmer JD, Raval R, Ong S, et al. Characterizing benefit from temozolomide in MGMT promoter unmethylated and methylated glioblastoma: a systematic review and meta-analysis. Neuro-oncology Adv. 2020;2:vdaa082.
11. Struve N, Binder ZA, Stead LF, Brend T, Bagley SJ, Faulkner C, et al. EGFRvIII upregulates DNA mismatch repair resulting in increased temozolomide sensitivity of MGMT promoter methylated glioblastoma. Oncogene. 2020;39:3041–55.
12. Brennan CW, Verhaak RGW, McKenna A, Campos B, Noushmehr H, Salama SR, et al. The somatic genomic landscape of glioblastoma. Cell. 2013;155:462–77.
13. Verhaak RGW, Hoadley KA, Purdom E, Wang V, Qi Y, Wilkerson MD, et al. Integrated genomic analysis identifies clinically relevant subtypes of glioblastoma characterized by abnormalities in PDGFRA, IDH1, EGFR, and NF1. Cancer Cell. 2010;17:98–110.
14. Li J, Liang R, Song C, Xiang Y, Liu Y. Prognostic significance of epidermal growth factor receptor expression in glioma patients. Oncotargets Ther. 2018;11:731–42.
15. Sur I, Taipale J. The role of enhancers in cancer. Nat Rev Cancer. 2016;16:483–93.
16. Remeseiro S, Hörnblad A, Spitz F. Gene regulation during development in the light of topologically associating domains. WIREs Dev Biol. 2016;5:169–85.
17. Schoenfelder S, Fraser P. Long-range enhancer-promoter contacts in gene expression control. Nat Rev Genet. 2019;55:5.
18. Zaugg JB, Sahlén P, Andersson R, Alberich-Jorda M, Laat W de, Deplancke B, et al. Current challenges in understanding the role of enhancers in disease. Nat Struct Mol Biol. 2022;29:1148–58.
19. Dakhel S, Davies WIL, Joseph JV, Tomar T, Remeseiro S, Gunhaga L. Chick fetal organ spheroids as a model to study development and disease. BMC Mol Cell Biol. 2021;22:37–17.
20. Melin BS, Barnholtz-Sloan JS, Wrensch MR, Johansen C, Il'yasova D, Kinnersley B, et al. Genome-wide association study of glioma subtypes identifies specific differences in genetic susceptibility to glioblastoma and non-glioblastoma tumors. Nat Genet. 2017;49:789–94.
21. Warburg O. Über den Stoffwechsel der Carcinomzelle. Naturwissenschaften. 1924;12:1131–7.
22. Liberti MV, Locasale JW. The Warburg effect: how does it benefit cancer cells? Trends Biochem Sci. 2016;41:211–8.
23. DeBerardinis RJ, Chandel NS. We need to talk about the Warburg effect. Nat Metabolism. 2020;2:127–9.
24. Sies H, Jones DP. Reactive oxygen species (ROS) as pleiotropic physiological signalling agents. Nat Rev Mol Cell Bio. 2020;21:363–83.
25. Azad N, Iyer AKV. Systems Biology of Free Radicals and Antioxidants. 2014. p. 113–35.
26. Cheung EC, Vousden KH. The role of ROS in tumour development and progression. Nat Rev Cancer. 2022;22:280–97.
27. Ge T, Gu X, Jia R, Ge S, Chai P, Zhuang A, et al. Crosstalk between metabolic reprogramming and epigenetics in cancer: updates on mechanisms and therapeutic opportunities. Cancer Commun. 2022;42:1049–82.
28. Dai Z, Ramesh V, Locasale JW. The evolving metabolic landscape of chromatin biology and epigenetics. Nat Rev Genet. 2020;21:737–53.
29. Shireman JM, Atashi F, Lee G, Ali ES, Saathoff MR, Park CH, et al. De novo purine biosynthesis is a major driver of chemoresistance in glioblastoma. Brain. 2021;144:1230–46.
30 Miska J, Rashidi A, Lee-Chang C, Gao P, Lopez-Rosas A, Zhang P, et al. Polyamines drive myeloid cell survival by buffering intracellular pH to promote immunosuppression in glioblastoma. Sci Adv. 2021;7:eabc8929.
31. Zhan Q, Yi K, Cui X, Li X, Yang S, Wang Q, et al. Blood exosomes-based targeted delivery of cPLA2 siRNA and metformin to modulate glioblastoma energy metabolism for tailoring personalized therapy. Neuro-Oncol. 2022;24:1871–83.
32. Roussos ET, Condeelis JS, Patsialou A. Chemotaxis in cancer. Nat Rev Cancer. 2011;11:573–87.
33. Wang G, Zhong K, Wang Z, Zhang Z, Tang X, Tong A, et al. Tumor-associated microglia and macrophages in glioblastoma: From basic insights to therapeutic opportunities. Front Immunol. 2022;13:964898.
34. Coniglio SJ, Eugenin E, Dobrenis K, Stanley ER, West BL, Symons MH, et al. Microglial stimulation of glioblastoma invasion involves Epidermal Growth Factor Receptor (EGFR) and Colony Stimulating Factor 1 Receptor (CSF-1R) Signaling. Mol Med. 2012;18:519–27.
35. Hobbs J, Nikiforova MN, Fardo DW, Bortoluzzi S, Cieply K, Hamilton RL, et al. Paradoxical relationship between the degree of EGFR amplification and outcome in glioblastomas. Am J Surg Pathology. 2012;36:1186–93.
36. Weller M, Butowski N, Tran DD, Recht LD, Lim M, Hirte H, et al. Rindopepimut with temozolomide for patients with newly diagnosed, EGFRvIII-expressing glioblastoma (ACT IV): a randomised, double-blind, international phase 3 trial. Lancet Oncol. 2017;18:1373–85.
37. Lin B, Ziebro J, Smithberger E, Skinner KR, Zhao E, Cloughesy TF, et al. EGFR, the Lazarus target for precision oncology in glioblastoma. Neuro-Oncol. 2022;24:2035–62.


## Publisher's Note

Springer Nature remains neutral with regard to jurisdictional claims in published maps and institutional affiliations.

**Ready to submit your research? Choose BMC and benefit from:**

- fast, convenient online submission
- thorough peer review by experienced researchers in your field
- rapid publication on acceptance
- support for research data, including large and complex data types
- gold Open Access which fosters wider collaboration and increased citations
- maximum visibility for your research: over 100M website views per year

**At BMC, research is always in progress.**

**Learn more** biomedcentral.com/submissions